Impact of Time-Selective Fading on the Performance of Quasi-Orthogonal Space–Time-Coded OFDM Systems

Yu Zhang, *Student Member, IEEE,* and Huaping Liu, *Member, IEEE*

***Abstract*—In this paper, we study the impact of time-selective fading on quasi-orthogonal space-time (ST) coded orthogonal frequency-division multiplexing (OFDM) systems over frequency-selective Rayleigh fading channels. OFDM is robust against frequency-selective fading, but it is more vulnerable to time-selective fading than single-carrier systems. In ST-OFDM, channel time variations cause not only intercarrier interference among different subcarriers in one OFDM symbol, but also inter-transmit-antenna interference. We quantify the impact of time-selective fading on the performance of quasi-orthogonal ST-OFDM systems by deriving, via an analytical approach, the expressions of carrier-to-interference and signal-to-interference-plus-noise ratios. We observe that system error performance is insensitive to changes in vehicle speeds and the channel power-delay profile, but very sensitive to changes in the number of subcarriers. We also evaluate the performance of five different detection schemes in the presence of time-selective fading. We show that although there exist differences in their relative performances, all these detection schemes suffer from an irreducible error floor.**

***Index Terms*—Intertransmit-antenna interference (ITAI), intercarrier interference (ICI), orthogonal frequency-division multiplexing (OFDM), space-time (ST) codes (STC), time-selective fading.**

I. Introduction

MOBILE wireless channels exhibit time-varying multipath fading, the rapidity of which can be quantified by the Doppler shift. Orthogonal frequency-division multiplexing (OFDM) is effective in avoiding intersymbol interference (ISI) that multipath delay might cause. However, it is sensitive to time-selective fading, which destroys the orthogonality among different subcarriers in one OFDM symbol, causing intercarrier interference (ICI) [1], [2].

Space–time (ST) coding (STC) is a technique to achieve transmit diversity in a multiantenna system by coding across both space and time domains [3]. Orthogonal ST block codes (STBCs) were originally proposed in [4] for systems with two transmit antennas. The orthogonal design was then generalized to systems with an arbitrary number of transmit antennas [5]. Since complex orthogonal STBCs with full spatial diversity and full transmission rate do not exist for more than two transmit antennas [5], quasi-orthogonal design with rate one but partial diversity was investigated in [6] and [7]. Recently, quasi-orthogonal STBC with constellation rotation was proposed in [8], [9] to provide full diversity. STBCs are typically designed assuming a quasi-static channel, and time-selective fading will cause intertransmit-antenna interference (ITAI) in orthogonal codes [10]. For quasi-orthogonal codes, channel time variations cause ITAI among all symbols,[1] and the pairwise maximum-likelihood (ML) decoding scheme [8] becomes suboptimal. To mitigate ITAI caused by channel time variations, many schemes have been studied: a simplified linear quasi-ML decoder for orthogonal STBC with two transmit antennas was proposed to cancel ITAI when the channel varies from one signaling interval to another [11]; a low-complexity receiver was proposed to lower the bit-error rate (BER) floor of orthogonal STBC with four transmit antennas using the conventional ML decoding method [12]; and a two-step zero-forcing (TS-ZF) scheme was applied to cancel ITAI and to eliminate the error floor of quasi-orthogonal STBC [13].

Multiple antennas can be combined with OFDM to achieve spatial diversity and/or to increase spectral efficiency through spatial multiplexing [14]. For multiantenna OFDM systems in frequency-selective environments, STC schemes must be extended to include the frequency element, forming ST-coded OFDM (ST-OFDM) [15], [16]. Similar to single-antenna OFDM, ST-OFDM is also sensitive to the Doppler shift and frequency errors which destroy the orthogonality among subcarriers, causing ICI [17]. In OFDM systems with N_s subcarriers, the OFDM symbol duration could be N_s times of the data symbol period. Consequently, ITAI caused by channel time variations in ST-OFDM systems is more pronounced than in common STC systems.

While the problems caused by time-selective fading in ST-OFDM have been recognized, the exact quantitative impact has not been well understood yet. In this paper, we analyze, via mainly an analytical approach, the impact of both ICI and ITAI to the performance of quasi-orthogonal ST-OFDM systems in the presence of time-selective Rayleigh fading. We also compare five detection schemes: the ZF scheme [18]; the TS-ZF scheme [13]; the minimum mean-squared error (MMSE) scheme [18]; the decorrelating decision-feedback (DF) scheme [19]; and the MMSE-DF scheme [20], and evaluate their symbol-error rate (SER) floors. This paper is

Paper approved by I. Lee, the Editor for Wireless Communication Theory of the IEEE Communications Society. Manuscript received December 14, 2004; revised April 22, 2005 and July 11, 2005.

The authors are with the School of Electrical Engineering and Computer Science, Oregon State University, Corvallis, OR 97331 USA (e-mail: zhangyu@eecs.orst.edu; hliu@eecs.oregonstate.edu).

Digital Object Identifier 10.1109/TCOMM.2005.863773

[1]With a quasi-static fading model, ITAI exists only between pairs of symbols with the 4×4 codes given in [8].

organized as follows. Section II provides the ST-OFDM system model. Analysis of the impact of ICI and ITAI is detailed in Section III. Simulation results are given in Section IV, followed by concluding remarks in Section V.

II. System Model

We focus on an STBC OFDM system with P transmit antennas, one receive antenna, and N_s subcarriers in a time-selective Rayleigh fading environment. Input symbols $\{a(i)\}$ are assumed to have the following properties:

$$E[a(i)] = 0$$
$$E[a(i)a^*(j)] = \begin{cases} 1, & i = j \\ 0, & i \neq j \end{cases}$$

where $(\cdot)^*$ and $E[\cdot]$ denote complex conjugate and expectation, respectively. The input sequence $\{a(i), i = 0, \ldots, N_sP - 1\}$ is serial-to-parallel converted into P sequences, each of length N_s, as

$$a_p(k) = a(k + (p-1)N_s) \qquad p = 1, \ldots, P, \quad k = 0, \ldots, N_s - 1. \quad (1)$$

Each of the N_s sequences $\{a_1(k), \ldots, a_P(k)\}$, $k = 0, \ldots, N_s - 1$, is mapped to a matrix $\boldsymbol{\Psi}_k$ of size $P \times P$ by using a quasi-orthogonal STBC scheme (e.g., the 4×4 quasi-orthogonal scheme given in [8]).

Then we take the inverse discrete Fourier transform (IDFT) of $\{\boldsymbol{\Psi}_0, \ldots, \boldsymbol{\Psi}_{N_s-1}\}$, forming the transmitted signals as[2]

$$\boldsymbol{S}_m = \frac{1}{\sqrt{N_s}} \sum_{k=0}^{N_s-1} \boldsymbol{\Psi}_k \cdot e^{j(2\pi/N_s)mk}, \quad m = 0, \ldots, N_s - 1. \quad (2)$$

Note that $\boldsymbol{S}_m$ is a $P \times P$ matrix, which represents the transmitted signals on the mth subcarrier. If we define

$$\boldsymbol{\Psi} = [\boldsymbol{\Psi}_0^T, \ldots, \boldsymbol{\Psi}_{N_s-1}^T]^T, \quad (N_sP \times P) \quad (3a)$$
$$\boldsymbol{S} = [\boldsymbol{S}_0^T, \ldots, \boldsymbol{S}_{N_s-1}^T]^T, \quad (N_sP \times P) \quad (3b)$$

where $(\cdot)^T$ denotes transpose, then $\boldsymbol{S}$ can be written as

$$\boldsymbol{S} = (\boldsymbol{U} \otimes \boldsymbol{I}_P)^H \boldsymbol{\Psi} \quad (4)$$

where $(\cdot)^H$ denotes complex conjugate transpose, $\otimes$ denotes Kronecker product, $\boldsymbol{I}_P$ is the $P \times P$ identity matrix, and $\boldsymbol{U}$ is the $N_s \times N_s$ unitary discrete Fourier transform (DFT) matrix given by

$$\boldsymbol{U} = \frac{1}{\sqrt{N_s}} \begin{bmatrix} 1 & 1 & \cdots & 1 \\ \vdots & \vdots & \ddots & \vdots \\ 1 & e^{-j(2\pi/N_s)(N_s-1)} & \cdots & e^{-j(2\pi/N_s)(N_s-1)(N_s-1)} \end{bmatrix}. \quad (5)$$

In frequency-selective fading channels with L resolvable paths, there exists interblock interference (IBI). To minimize this IBI, a cyclic prefix of length c_p ($c_p \geq L$) is added to each OFDM symbol. In the receiver, the cyclic prefix is discarded, leaving IBI-free, information-bearing signals. Combined with the characteristics of time-selective fading, the $N_s \times N_sP$ spatiotemporal channel matrix $\boldsymbol{H}_t$ is given by (6) at the bottom of the page,[3] where L is less than or equal to N_s, $\boldsymbol{0}$ is a $P \times 1$ zero vector, and each nonzero block of $\boldsymbol{H}_t$ contains the $P \times 1$ channel vector $\boldsymbol{h}_{t,l}(n)$ for a particular path l at time nT_s (T_s is the data symbol period) expressed as

$$\boldsymbol{h}_{t,l}(n) = [h_{t,1,l}(n), \ldots, h_{t,P,l}(n)]^T, \qquad l = 0, \ldots, L-1, n = 0, \ldots, N_s - 1. \quad (7)$$

In the case of quasi-static fading[4] that allows the channel coefficients to be constant over an OFDM symbol period and change independently from one symbol to another, $\boldsymbol{H}_t$ has a block-circulant structure. Without loss of generality, we omit the index of OFDM symbol period t in the following discussion.

Assuming a wide sense stationary uncorrelated scattering (WSSUS) channel [17], all elements of $\boldsymbol{h}_l(n)$ are modeled as independent complex Gaussian random variables with zero mean and equal variance. Let the power of the first path $\boldsymbol{h}_0(n)$ be normalized, i.e., all elements of $\boldsymbol{h}_0(n)$ have unit variance. The model of the channel with L resolvable multipath components can be expressed as [21, eq. (2)]

$$h(\tau) = \sum_{l=0}^{L-1} \rho_l \delta(\tau - \tau_l T_s) \quad (8)$$

where ρ_l is the zero-mean complex Gaussian random variable, and τ_l is the delay of the lth path normalized with respect to T_s. The delays $\{\tau_l\}$ are assumed to be uniformly distributed over the cyclic prefix c_p. The channel has an exponential power-delay profile $\theta(\tau_l) = e^{-\tau_l/\tau_{\mathrm{rms}}}$, where τ_{rms} represents the root-mean-

[2]Note that this is not the only way to construct ST-OFDM. We adopt it because of its mathematical convenience. Implementation of this scheme requires $P \times P$ IDFT operations. If IDFT is done before STBC mapping, then only P IDFT operations are needed.

[3]The index in the parenthesis following $\boldsymbol{h}_{t,l}$ is the time index.

[4]Quasi-static fading models are appropriate to describe slow-fading channels.

$$\boldsymbol{H}_t = \begin{bmatrix} \boldsymbol{h}_{t,0}^T(0) & \cdots & \boldsymbol{0}^T & \boldsymbol{h}_{t,L-1}^T(0) & \cdots & \boldsymbol{h}_{t,1}^T(0) \\ \vdots & & & \vdots & & \vdots \\ \boldsymbol{h}_{t,L-1}^T(L-1) & \cdots & \boldsymbol{h}_{t,1}^T(L-1) & \boldsymbol{h}_{t,0}^T(L-1) & \cdots & \boldsymbol{0}^T \\ \vdots & & & \vdots & & \vdots \\ \boldsymbol{0}^T & \cdots & \boldsymbol{h}_{t,L-1}^T(N_s-1) & \cdots & \boldsymbol{h}_{t,1}^T(N_s-1) & \boldsymbol{h}_{t,0}^T(N_s-1) \end{bmatrix} \quad (6)$$

square (rms) delay spread, which is also normalized with respect to T_s. Since the channel is time-varying, the relationship between the channel coefficients for path l of antenna p at times nT_s and $(n+m)T_s$ can be described by using a first-order autoregressive model as [11], [22]

$$h_{p,l}(n+m) = \alpha_m h_{p,l}(n) + \beta_{p,l}(n+m) \tag{9}$$

where

$$\alpha_m = \frac{E\left[h_{p,l}(n)\cdot h^*_{p,l}(n+m)\right]}{e^{-\tau_l/\tau_{\rm rms}}} = J_0(2\pi m f_d T_s) \tag{10}$$

where f_d is the Doppler shift, $J_0(\cdot)$ is the zeroth-order Bessel function of the first kind, and $\beta_{p,l}(n)$ are independent (for different indexes p, l, and n) complex Gaussian random variables with zero mean and variance

$$\sigma^2_\beta = \begin{cases} 1-\alpha_m^2, & l=0 \\ e^{-\tau_l/\tau_{\rm rms}}(1-\alpha_m^2), & l\neq 0. \end{cases} \tag{11}$$

The received signals is expressed in an $N_s \times P$ matrix as

$$\boldsymbol{R} = \boldsymbol{H}\boldsymbol{S} + \boldsymbol{V} \tag{12}$$

where $\boldsymbol{V} = [\boldsymbol{v}_0, \ldots, \boldsymbol{v}_{N_s-1}]^T$ $(N_s \times P)$ is the additive white Gaussian noise (AWGN) matrix whose elements are independent and identically distributed (i.i.d.). Hence

$$E[\vec{(}\boldsymbol{V}) \cdot \vec{(}\boldsymbol{V})^H] = \sigma^2 \boldsymbol{I}_{N_s P} \tag{13}$$

where $\vec{(}\boldsymbol{V})$ is the vector obtained by vertically stacking the columns of matrix $\boldsymbol{V}$, and σ^2 is the variance of the zero-mean noise samples when the transmitted symbol energy is normalized to unity.

In the special case of a quasi-static fading, $\boldsymbol{h}_l(n) = \boldsymbol{h}_l$, $n = 0, \ldots, N_s-1$. Thus, $\boldsymbol{H}$ becomes a block-circulant matrix and has the following eigendecomposition:

$$\boldsymbol{H} = \boldsymbol{U}^H \boldsymbol{\Lambda}(\boldsymbol{U} \otimes \boldsymbol{I}_P) \tag{14}$$

where $N_s \times N_s P$ matrix $\boldsymbol{\Lambda} = \mathrm{diag}[\boldsymbol{\lambda}_0^T, \ldots, \boldsymbol{\lambda}_{N_s-1}^T]$ is a block-diagonal matrix whose (k,k)th block is given by

$$\boldsymbol{\lambda}_k = \sum_{l=0}^{L-1} \boldsymbol{h}_l \cdot e^{-j(2\pi/N_s)k\boldsymbol{l}}, \quad k = 0, \ldots, N_s-1. \tag{15}$$

Analysis of the receiver under quasi-static fading is straightforward. The received signal $\boldsymbol{R}$ is processed by multiplying it with $\boldsymbol{U}$, forming $N_s \times P$ matrix $\boldsymbol{X}$ as

$$\begin{aligned} \boldsymbol{X} &= [\boldsymbol{x}_0, \ldots, \boldsymbol{x}_{N_s-1}]^T \\ &= \boldsymbol{U}\boldsymbol{R} = \boldsymbol{\Lambda}\boldsymbol{\Psi} + \boldsymbol{U}\boldsymbol{V} \end{aligned} \tag{16}$$

where $\boldsymbol{x}_k = [x_1(k), \ldots, x_P(k)]^T$. Let $\boldsymbol{w}_k = [w_1(k), \ldots, w_P(k)]^T$ and $\boldsymbol{W} = \boldsymbol{U}\boldsymbol{V} = [\boldsymbol{w}_0, \ldots, \boldsymbol{w}_{N_s-1}]^T$ $(N_s \times P)$. From (16), $\boldsymbol{x}_k$ can be obtained as

$$\boldsymbol{x}_k^T = \boldsymbol{\lambda}_k^T \boldsymbol{\Psi}_k + \boldsymbol{w}_k^T, \quad k = 0, \ldots, N_s-1 \tag{17}$$

where

$$\boldsymbol{w}_k = \frac{1}{\sqrt{N_s}} \sum_{m=0}^{N_s-1} \boldsymbol{v}_m \cdot e^{-j(2\pi/N_s)mk}. \tag{18}$$

Note that $\boldsymbol{W}$ has the same first- and second-order statistics as $\boldsymbol{V}$, i.e., all elements of $\boldsymbol{W}$ are i.i.d. with zero mean and variance σ^2. It is clear from (17) that ICI does not exist in the ST-OFDM system over quasi-static channels.

The P symbols in each column of $\boldsymbol{\Psi}_k$ are transmitted from the P transmit antennas simultaneously during every OFDM symbol period. If the channel is time-invariant over P consecutive OFDM symbol periods, the pairwise ML scheme [8] can be used to detect pairs of transmitted symbols, instead of symbol by symbol, and there is no error floor in BER performance.

III. Impact of Time-Varying Fading

A. CIR and SINR in the Presence of Time-Varying Fading

For OFDM systems over fast-fading channels, channel estimation is generally carried out by transmitting pilot symbols in given positions of the frequency-time grid [23], [24]. We assume hereafter that channel-state information (CSI) is known in the receiver. In the presence of time-selective fading, $\boldsymbol{H}$ is no longer a block-circulant matrix. Consequently, $\boldsymbol{G} = \boldsymbol{U}\boldsymbol{H}(\boldsymbol{U}\otimes\boldsymbol{I}_P)^H$ is no longer a block-diagonal matrix as $\boldsymbol{\Lambda}$ given in (14). This shows that time-selective fading causes ICI, which is represented by the off-diagonal blocks of $\boldsymbol{G}$. For this more general case, we can rewrite (16) as

$$\boldsymbol{X} = [\boldsymbol{x}_0, \ldots, \boldsymbol{x}_{N_s-1}]^T = \boldsymbol{G}\boldsymbol{\Psi} + \boldsymbol{W} \tag{19}$$

where

$$\boldsymbol{x}_k^T = \boldsymbol{g}_{k,k}^T \boldsymbol{\Psi}_k + \sum_{k'=0, k'\neq k}^{N_s-1} \boldsymbol{g}_{k,k'}^T \boldsymbol{\Psi}_{k'} + \boldsymbol{w}_k^T, \quad k = 0, \ldots, N_s-1 \tag{20}$$

and $\boldsymbol{g}_{k,k'} = [g_{k,k'}^{(1)}, \ldots, g_{k,k'}^{(P)}]^T$, $k, k' = 0, \ldots, N_s-1$, is the (k,k')th block of $\boldsymbol{G}$. Apparently, the second term on the right-hand side of (20) represents ICI.

To make the rest of the analysis in this paper clearer and easier to understand, we focus on using the 4×4 (i.e., $P=4$) quasi-orthogonal STBC with constellation rotation given in [8], which is replicated here as

$$\boldsymbol{\Psi}_k = \begin{bmatrix} a_1(k) & -a_2^*(k) & e^{j\phi}a_3(k) & -e^{-j\phi}a_4^*(k) \\ a_2(k) & a_1^*(k) & e^{j\phi}a_4(k) & e^{-j\phi}a_3^*(k) \\ e^{j\phi}a_3(k) & -e^{-j\phi}a_4^*(k) & a_1(k) & -a_2^*(k) \\ e^{j\phi}a_4(k) & e^{-j\phi}a_3^*(k) & a_2(k) & a_1^*(k) \end{bmatrix} \tag{21}$$

where the rotation angle ϕ depends on the signal constellation. The analysis procedures and conclusions drawn for this specific case can be easily extended to different numbers of antennas and code structures (e.g., the 8×8 code in [8]).

ICI can be well quantified by using the carrier-to-interference ratio (CIR) [25]. In order to quantify the effects of time-varying fading, we derive CIR as a function of the number of subcarriers and the normalized Doppler shift $(f_d T_s)$. Let us define three vectors

$$\begin{aligned} \boldsymbol{y}_k &= [x_1(k), x_2^*(k), x_3(k), x_4^*(k)]^T \\ \boldsymbol{z}_k &= [w_1(k), w_2^*(k), w_3(k), w_4^*(k)]^T \\ \boldsymbol{\psi}_k &= [a_1(k), a_2(k), e^{j\phi}a_3(k), e^{j\phi}a_4(k)]^T. \end{aligned}$$

From (20), $\boldsymbol{y}_k$ can be expressed as

$$\boldsymbol{y}_k = \boldsymbol{M}_{k,k}\boldsymbol{\psi}_k + \sum_{k'=0,k'\neq k}^{N_s-1} \boldsymbol{M}_{k,k'}\boldsymbol{\psi}_{k'} + \boldsymbol{z}_k \tag{22}$$

where

$$\boldsymbol{M}_{k,k'} = \begin{bmatrix} \boldsymbol{M}_{k,k'}^{(1,2)}(0) & \boldsymbol{M}_{k,k'}^{(3,4)}(0) \\ \boldsymbol{M}_{k,k'}^{(3,4)}(2(N_s+c_p)) & \boldsymbol{M}_{k,k'}^{(1,2)}(2(N_s+c_p)) \end{bmatrix} \quad k,k' = 0,\ldots,N_s-1 \tag{23}$$

with

$$\boldsymbol{M}_{k,k'}^{(i,j)}(n) = \begin{bmatrix} g_{k,k'}^{(i)}(n) & g_{k,k'}^{(j)}(n) \\ g_{k,k'}^{(j)*}(n+N_s+c_p) & -g_{k,k'}^{(i)*}(n+N_s+c_p) \end{bmatrix}. \tag{24}$$

By letting $g_{k,k'}^{(p)}(0) = g_{k,k'}^{(p)}$, $p = 1,\ldots,4$, we have

$$g_{k,k'}^{(p)}(q(N_s+c_p)) = J_0(2\pi f_d(N_s+c_p)T_s) \times g_{k,k'}^{(p)}[(q-1)(N_s+c_p)] + \varepsilon_{k,k'}^{(p)}(q(N_s+c_p)) \tag{25}$$

where $\{\varepsilon_{k,k'}^{(p)}(q(N_s+c_p)), q=1,2,3\}$ are independent complex Gaussian random variables with zero mean and variance

$$\sigma_{\varepsilon_{k,k'}}^2 = (1 - J_0^2(2\pi f_d(N_s+c_p)T_s)) \cdot \mathrm{var}(g_{k,k'}^{(p)}) \tag{26}$$

where $\mathrm{var}(\cdot)$ denotes variance. Note that the spaced-time correlation function (10) is for channel coefficients in the time domain. In obtaining (25) in the frequency domain, we have applied the time-frequency relationship $\boldsymbol{G} = \boldsymbol{U}\boldsymbol{H}(\boldsymbol{U}\otimes\boldsymbol{I}_P)^H$ and (9) and (10).

Let $\boldsymbol{\Upsilon}$ be an $N_s \times N_s$ matrix given by

$$\boldsymbol{\Upsilon} = \begin{bmatrix} \mathrm{var}(g_{0,0}^{(p)}) & \cdots & \mathrm{var}(g_{0,N_s-1}^{(p)}) \\ \vdots & \ddots & \vdots \\ \mathrm{var}(g_{N_s-1,0}^{(p)}) & \cdots & \mathrm{var}(g_{N_s-1,N_s-1}^{(p)}) \end{bmatrix}. \tag{27}$$

As shown in the Appendix, for a particular antenna index p, $\boldsymbol{\Upsilon}$ has a circulant structure as

$$\boldsymbol{\Upsilon} = \begin{bmatrix} \gamma_0 & \gamma_1 & \cdots & \gamma_{N_s-1} \\ \gamma_{N_s-1} & \gamma_0 & \cdots & \gamma_{N_s-2} \\ \vdots & \vdots & & \vdots \\ \gamma_1 & \gamma_2 & \cdots & \gamma_0 \end{bmatrix}. \tag{28}$$

Since elements of $\boldsymbol{g}_{k,k'}$ are i.i.d. Gaussian random variables [17], (28) applies to all antennas. It is also shown in the Appendix that $\gamma_{k'}$ defined in (28) can be expressed in closed form as

$$\gamma_{k'} = \frac{1}{N_s^2} \times \sum_{l=0}^{L-1}\left[N_s + 2\sum_{i=1}^{N_s-1}(N_s-i)\,\alpha_i \cos\left(\frac{2\pi}{N_s}k'i\right)\right] \times e^{-\tau_l/\tau_{\mathrm{rms}}}, \quad k' = 0,\ldots,N_s-1. \tag{29}$$

With (29), $g_{k,k'}^{(p)}(q(N_s+c_p))$ in (25) can be obtained by substituting $\gamma_{k'}$ into (26). As a result of channel time variations, $\gamma_{k'} \neq 0$ for $k' \neq 0$, which causes ICI. In the presence of time-varying fading, CIR for quasi-orthogonal STBC given in (21) applied in an OFDM system is obtained as

$$\begin{aligned} \mathrm{CIR} &= \frac{E\left[\|\boldsymbol{M}_{k,k}\boldsymbol{\psi}_k\|_F^2\right]}{E\left[\left\|\sum_{\substack{k'=0\\k'\neq k}}^{N_s-1}\boldsymbol{M}_{k,k'}\boldsymbol{\psi}_{k'}\right\|_F^2\right]} \\ &= \frac{tr\left\{E\left[\boldsymbol{M}_{k,k}\boldsymbol{\psi}_k\boldsymbol{\psi}_k^H\boldsymbol{M}_{k,k}^H\right]\right\}}{tr\left\{E\left[\left(\sum_{\substack{k'=0\\k'\neq k}}^{N_s-1}\boldsymbol{M}_{k,k'}\boldsymbol{\psi}_{k'}\right)\left(\sum_{\substack{k'=0\\k'\neq k}}^{N_s-1}\boldsymbol{M}_{k,k'}\boldsymbol{\psi}_{k'}\right)^H\right]\right\}} \\ &= \frac{E\left[\sum_{q=0}^{3}\sum_{p=1}^{4}|g_{k,k}^{(p)}(q(N_s+c_p))|^2\right]}{E\left[\sum_{\substack{k'=0\\k'\neq k}}^{N_s-1}\sum_{q=0}^{3}\sum_{p=1}^{4}|g_{k,k'}^{(p)}(q(N_s+c_p))|^2\right]} \\ &= \frac{\gamma_0}{\sum_{k'=1}^{N_s-1}\gamma_{k'}} \\ &= \frac{N_s + 2\sum_{i=1}^{N_s-1}(N_s-i)J_0(2\pi i f_d T_s)}{\sum_{k'=1}^{N_s-1}\left[N_s + 2\sum_{i=1}^{N_s-1}(N_s-i)J_0(2\pi i f_d T_s)\cos\left(\frac{2\pi}{N_s}k'i\right)\right]} \end{aligned} \tag{30}$$

where $\|\cdot\|_F$ denotes the Frobenius norm and $tr(\cdot)$ denotes the trace of a matrix. In deriving the fourth equality of (30), we have applied the property that $g_{k,k'}^{(p)}(q(N_s+c_p))$, $p=1,\ldots,4$, have the same variance. Note that CIR is independent of the channel power-delay profile and the number of resolvable paths. Furthermore, the signal-to-interference-plus-noise ratio (SINR) of this quasi-orthogonal ST-OFDM system is obtained as

$$\begin{aligned} \mathrm{SINR} &= \frac{E\left[\|\boldsymbol{M}_{k,k}\boldsymbol{\psi}_k\|_F^2\right]}{E\left[\left\|\sum_{\substack{k'=0\\k'\neq k}}^{N_s-1}\boldsymbol{M}_{k,k'}\boldsymbol{\psi}_{k'} + \boldsymbol{z}_k\right\|_F^2\right]} \\ &= \frac{tr\left\{E\left[\boldsymbol{M}_{k,k}\boldsymbol{\psi}_k\boldsymbol{\psi}_k^H\boldsymbol{M}_{k,k}^H\right]\right\}}{tr\left\{E\left[\left(\sum_{\substack{k'=0\\k'\neq k}}^{N_s-1}\boldsymbol{M}_{k,k'}\boldsymbol{\psi}_{k'}\right)\left(\sum_{\substack{k'=0\\k'\neq k}}^{N_s-1}\boldsymbol{M}_{k,k'}\boldsymbol{\psi}_{k'}\right)^H + \boldsymbol{z}_k\boldsymbol{z}_k^H\right]\right\}} \\ &= \frac{4\gamma_0}{4\sum_{k'=1}^{N_s-1}\gamma_{k'} + \sigma^2} \end{aligned} \tag{31}$$

where $\gamma_{k'}$ was given in (29). Moreover, the channel time variations over four consecutive OFDM symbols, as seen in the 4×4

matrix $\boldsymbol{M}_{k,k'}$ given in (23) introduce, as mentioned in Section I, additional ITAI among elements of $\boldsymbol{\psi}_k$.

B. Detection

In a quasi-static fading channel, the received signal can be directly processed by a ST decoder. In a time-varying fading channel, detection could be done as follows. Let ICI and noise terms in (22) be represented by a single variable $\boldsymbol{d}_k$ as

$$\boldsymbol{d}_k = \sum_{k'=0,k'\neq k}^{N_s-1} \boldsymbol{M}_{k,k'}\boldsymbol{\psi}_{k'} + \boldsymbol{z}_k. \tag{32}$$

Various schemes have been proposed for detection of quasi-orthogonal STBC over time-selective fading channels. For example, a TS-ZF detector was proposed in [13], assuming perfect CSI in the receiver; an effective equalization technique based on the lattice representation of STBC schemes was derived and analyzed in [10]. The main objective of this scheme is to lower the error floor due to ITAI caused by channel time selectivity. However, quasi-orthogonal ST-OFDM systems over time-selective multipath fading channels not only suffer from ITAI, but also ICI, especially when N_s is large. Thus, the TS-ZF scheme will not be very effective for the system being addressed in this paper.

In a simpler ZF detector, $\boldsymbol{y}_k$ is processed as

$$\boldsymbol{\Theta}_k\boldsymbol{y}_k = \boldsymbol{\Theta}_k\boldsymbol{M}_{k,k}\boldsymbol{\psi}_k + \boldsymbol{\Theta}_k\boldsymbol{d}_k \tag{33}$$

where $\boldsymbol{\Theta}_k = \boldsymbol{M}_{k,k}^{-1}$. Then the least-square (LS) criterion can be used to detect the transmitted signal as

$$\widehat{a}_p(k) = \begin{cases} \underbrace{\arg\min}_{a(i)\in\boldsymbol{\mathcal{A}}} |[\boldsymbol{\Theta}_k]_p\boldsymbol{y}_k - a(i)|^2, & p=1,2 \\ \underbrace{\arg\min}_{a(i)\in\boldsymbol{\mathcal{A}}} |[\boldsymbol{\Theta}_k]_p\boldsymbol{y}_k - e^{j\phi}a(i)|^2, & p=3,4 \end{cases} \tag{34}$$

where $\boldsymbol{\mathcal{A}}$ is the symbol alphabet, and $[\boldsymbol{\Theta}_k]_p$ is the pth row of $\boldsymbol{\Theta}_k$.

When the MMSE detection scheme is applied, the cost function $E[\|\boldsymbol{\psi}_k - \acute{\boldsymbol{W}}_k^H\boldsymbol{y}_k\|_F^2]$ is minimized by finding an appropriate coefficient matrix $\acute{\boldsymbol{W}}_k$. With some algebraic manipulations, the optimal matrix is obtained as

$$\acute{\boldsymbol{W}}_k = \left(\boldsymbol{M}_{k,k}\boldsymbol{M}_{k,k}^H + \acute{\boldsymbol{N}}_k\right)^{-1}\boldsymbol{M}_{k,k} \tag{35}$$

where $\acute{\boldsymbol{N}}_k$ is given in (36) at the bottom of the page, with $\acute{J}_i = J_0(2\pi f_d i(N_s+c_p)T_s)$, $i=1,2,3$. Thus, the MMSE criterion is given by

$$\hat{\boldsymbol{\psi}}_k = \acute{\boldsymbol{W}}_k^H\boldsymbol{y}_k = \boldsymbol{M}_{k,k}^H\left(\boldsymbol{M}_{k,k}\boldsymbol{M}_{k,k}^H + \acute{\boldsymbol{N}}_k\right)^{-1}\boldsymbol{y}_k. \tag{37}$$

The decorrelating DF and the MMSE-DF schemes have been shown to provide better performance than the ZF and MMSE schemes [26]. In the decorrelating DF detection scheme, $\boldsymbol{y}_k$ is premultiplied by $\boldsymbol{\mathcal{L}}^{-1}\boldsymbol{M}_{k,k}^H$ as

$$\begin{aligned}\widetilde{\boldsymbol{y}}_k &= \boldsymbol{\mathcal{L}}^{-1}\boldsymbol{M}_{k,k}^H\boldsymbol{y}_k \\ &= \boldsymbol{\mathcal{L}}^{-1}\boldsymbol{M}_{k,k}^H\boldsymbol{M}_{k,k}\boldsymbol{\psi}_k + \boldsymbol{\mathcal{L}}^{-1}\boldsymbol{M}_{k,k}^H\boldsymbol{d}_k \\ &= \boldsymbol{\mathcal{L}}^H\boldsymbol{\psi}_k + \boldsymbol{e}_k\end{aligned} \tag{38}$$

where $\boldsymbol{\mathcal{L}}^H$ is an upper triangular matrix obtained by using the Cholesky decomposition as

$$\boldsymbol{\mathcal{R}} = \boldsymbol{M}_{k,k}^H\boldsymbol{M}_{k,k} = \boldsymbol{\mathcal{L}}\boldsymbol{\mathcal{L}}^H.$$

The pth component of $\widetilde{\boldsymbol{y}}_k$ is given by

$$[\widetilde{\boldsymbol{y}}_k]_p = \boldsymbol{\mathcal{L}}_{p,p}^H[\boldsymbol{\psi}_k]_p + \sum_{i=p+1}^{4}\boldsymbol{\mathcal{L}}_{p,i}^H[\boldsymbol{\psi}_k]_i + [\boldsymbol{e}_k]_p \tag{39}$$

which contains only interference from $(4-p)$ signals. The last component $[\widetilde{\boldsymbol{y}}_k]_4$ contains no interference, so a decision for this transmitted signal can be made first: $\widehat{a}_4(k) = \mathrm{dec}\{e^{-j\phi}[\widetilde{\boldsymbol{y}}_k]_4\}$, where $\mathrm{dec}(\cdot)$ is the slice function corresponding to the specific modulation scheme applied. The next signal can be detected by subtracting the interference contribution from the fourth signal using the previous decision as $\widehat{a}_3(k) = \mathrm{dec}\{e^{-j\phi}([\widetilde{\boldsymbol{y}}_k]_3 - \boldsymbol{\mathcal{L}}_{3,4}^H\widehat{a}_4(k)e^{j\phi})\}$. This procedure is repeated until all signals are detected. The MMSE-DF scheme is the one that minimizes the average energy of $[\widetilde{\boldsymbol{y}}_k]_p - a_p(k)$, $p=1,2$ and $[\widetilde{\boldsymbol{y}}_k]_p - e^{j\phi}a_p(k)$, $p=3,4$ under the assumption that previously detected signals in the feedback filter are correct. Details of this scheme can be found in [20] and [27].

IV. Simulation Results and Discussion

In simulations, we assume a system with four transmit antennas and one receive antenna, employing quaternary phase-shift keying (QPSK) modulation. The 4×4 quasi-orthogonal STBC given in [8] and replicated in (21) is applied ($\phi = \pi/4$ used in simulation). The time-selective Rayleigh fading channel is assumed to have three resolvable multipath components, and the channel Doppler shift is calculated based on a carrier frequency of $f_c = 2$ GHz.

Fig. 1 shows the impact of data symbol period T_s ($N_s = 12$) and vehicle speed on CIR by using the analytical expression given in (30). Note, again, that CIR does not depend on the power-delay profile of the channel. CIR curves are compared for three different vehicle speeds chosen as $v_s = 30$, 60, and 100 km/h, which are typical for urban and suburban environments. It is clearly observed that CIR is inversely proportional

$$\acute{\boldsymbol{N}}_k = \begin{bmatrix} 4\sum_{k'=1}^{N_s-1}\gamma_{k'} + \sigma^2 & 4\acute{J}_1\sum_{k'=1}^{N_s-1}\gamma_{k'} & 4\acute{J}_2\sum_{k'=1}^{N_s-1}\gamma_{k'} & 4\acute{J}_3\sum_{k'=1}^{N_s-1}\gamma_{k'} \\ 4\acute{J}_1\sum_{k'=1}^{N_s-1}\gamma_{k'} & 4\sum_{k'=1}^{N_s-1}\gamma_{k'} + \sigma^2 & 4\acute{J}_1\sum_{k'=1}^{N_s-1}\gamma_{k'} & 4\acute{J}_2\sum_{k'=1}^{N_s-1}\gamma_{k'} \\ 4\acute{J}_2\sum_{k'=1}^{N_s-1}\gamma_{k'} & 4\acute{J}_1\sum_{k'=1}^{N_s-1}\gamma_{k'} & 4\sum_{k'=1}^{N_s-1}\gamma_{k'} + \sigma^2 & 4\acute{J}_1\sum_{k'=1}^{N_s-1}\gamma_{k'} \\ 4\acute{J}_3\sum_{k'=1}^{N_s-1}\gamma_{k'} & 4\acute{J}_2\sum_{k'=1}^{N_s-1}\gamma_{k'} & 4\acute{J}_1\sum_{k'=1}^{N_s-1}\gamma_{k'} & 4\sum_{k'=1}^{N_s-1}\gamma_{k'} + \sigma^2 \end{bmatrix} \tag{36}$$

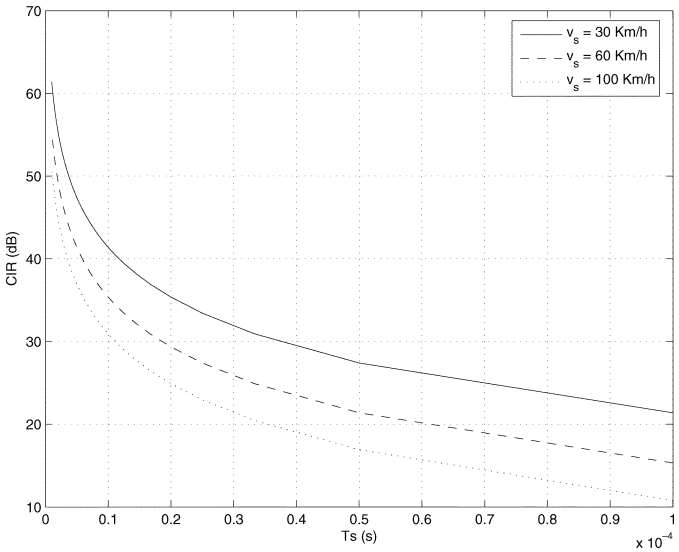

Fig. 1. CIR comparisons with different fading rates ($N_s = 12$).

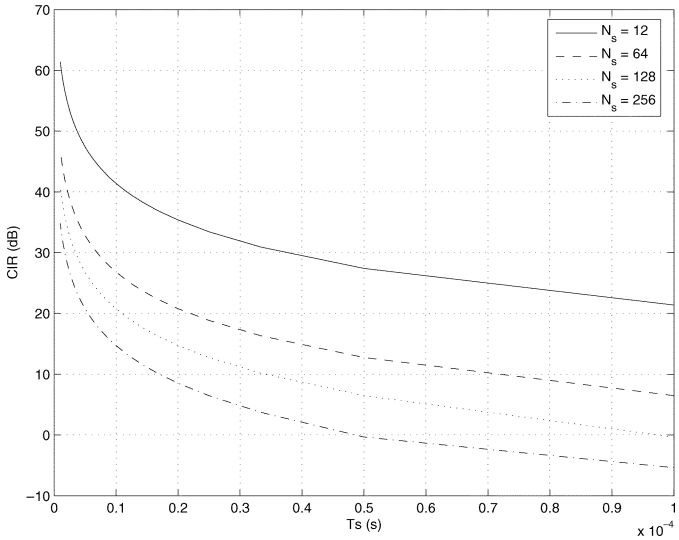

Fig. 2. CIR comparisons with different numbers of subcarriers ($v_s = 30$ km/h).

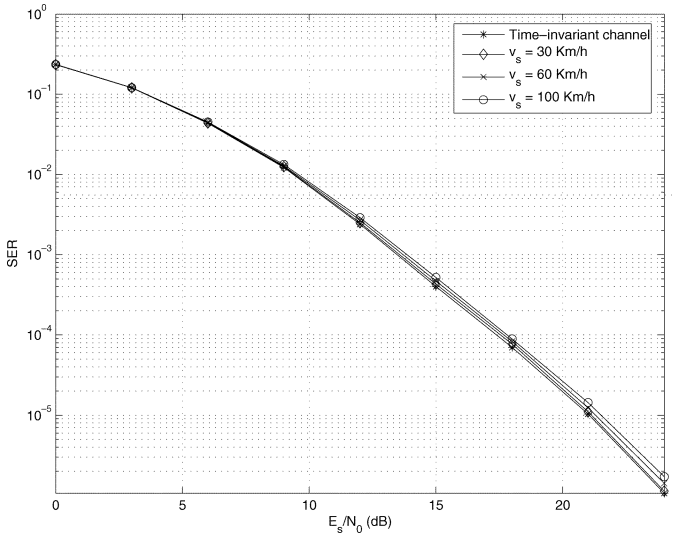

Fig. 3. SER versus E_s/N_0 for quasi-orthogonal ST-OFDM systems with different fading rates ($N_s = 12, T_s = 5 \times 10^{-7}$ s).

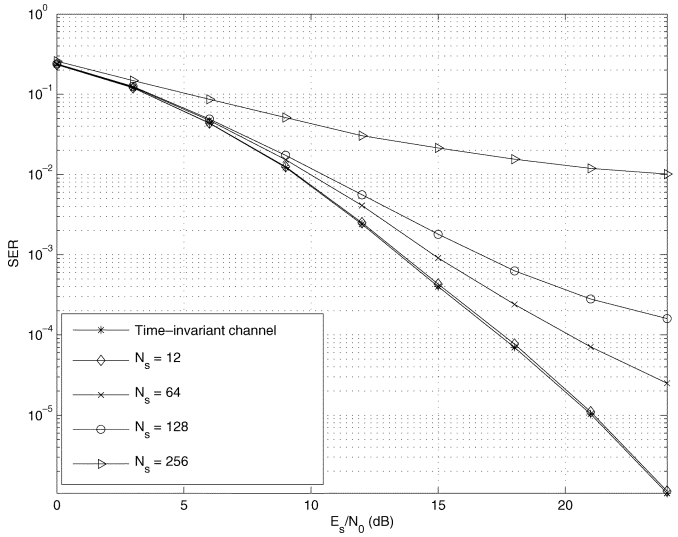

Fig. 4. SER versus E_s/N_0 for quasi-orthogonal ST-OFDM systems with different numbers of subcarriers ($v_s = 30$ km/h, $T_s = 5 \times 10^{-7}$ s).

to T_s and vehicle speed, which makes sense, as a larger value of T_s or v_s makes the quasi-orthogonal ST-OFDM system more vulnerable to time variations of the channel coefficients.

In Fig. 2, CIR curves of the system with $v_s = 30$ km/h and different numbers of subcarriers in one OFDM symbol ($N_s =$ 12, 64, 128, and 256) are obtained. It is observed that given the same data symbol duration T_s, CIR decreases significantly as the number of subcarriers increases.

Shown in Fig. 3 are the simulated SER performances of the system when a ZF detection scheme is employed. The power-delay profile-related parameters are $\tau_0 = 0$, $\tau_1 = 2$, $\tau_2 = 3$, and $\tau_{\rm rms} = 20$. The OFDM symbol is assumed to have $N_s = 12$ subcarriers, and the data symbol period is $T_s = 1/(2 \times 10^6)$ s. Performances with different vehicle speeds ($v_s = 30$, 60, and 100 km/h) are compared. In the same figure, the curve of the quasi-orthogonal ST-OFDM system over a time-invariant multipath fading channel is used as the baseline performance. When the number of subcarriers is small ($N_s = 12$ in Fig. 3), the system performs almost the same for any of the vehicle speeds applied, and they all approach the baseline performance. As the number of subcarriers increases, however, system performance deteriorates dramatically. This is clearly shown in Fig. 4, where the vehicle speed is $v_s = 30$ km/h, and all other parameters are the same as those applied to generate Fig. 3. From the SER versus E_s/N_0 curves with $N_s = 12$, 64, 128, and 256, it is observed that the error floor increases as N_s increases. The main reason is that a larger number of subcarriers within one OFDM symbol not only causes more severe ICI, but also increases the time interval ($(N_s + c_p)T_s$) in (26), causing a greater amount of ITAI within one STBC matrix.

In Figs. 3 and 4, the same exponential power-delay profile is applied. Fig. 5 shows the impact of different power-delay profiles on the SER performance. Three cases are simulated: 1) a

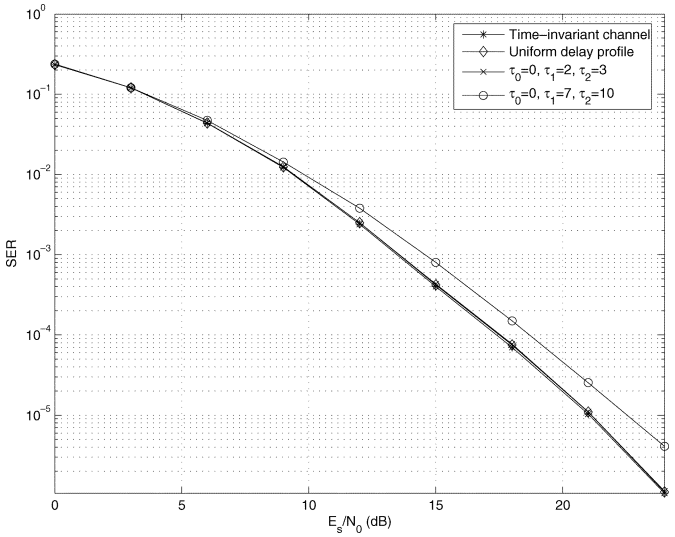

Fig. 5. SER versus E_s/N_0 for quasi-orthogonal ST-OFDM systems with different power-delay profiles ($N_s = 12$, $\tau_{\rm rms} = 10$, $v_s = 30$ km/h).

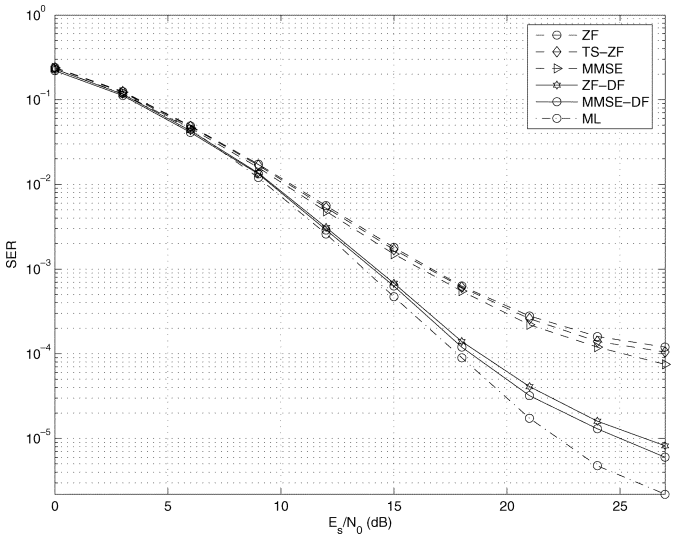

Fig. 6. SER versus E_s/N_0 for quasi-orthogonal ST-OFDM systems with different detection schemes ($N_s = 128$, $v_s = 30$ km/h, $T_s = 5 \times 10^{-7}$ s).

uniform power-delay profile as defined in [21, App. A], which results in unit variance of all elements of $\boldsymbol{H}$; 2) $\tau_0 = 0$, $\tau_1 = 2$, $\tau_2 = 3$; and 3) $\tau_0 = 0$, $\tau_1 = 7$, $\tau_2 = 10$. Other parameters applied are $\tau_{\rm rms} = 10$ for cases 2) and 3), $v_s = 30$ km/h, $N_s = 12$, and $T_s = 1/(2 \times 10^6)$ s. For comparison, the baseline performance curve shown in Figs. 3 and 4 is also shown in Fig. 5. For the set of channel parameters chosen, it seems that the channel profile only affects the system performance slightly.

In Fig. 6, we compare the performances of five different detection methods: the ZF, the TS-ZF, the MMSE, the decorrelating DF (also known as the ZF-DF), and the MMSE-DF schemes. Other than that $N_s = 128$, all other parameters are the same as those applied for Fig. 4. The ML scheme is used as the benchmark for other detection schemes. Since these schemes are not specifically optimized for ST-OFDM systems over time-varying fading channels for which ICI should be dealt

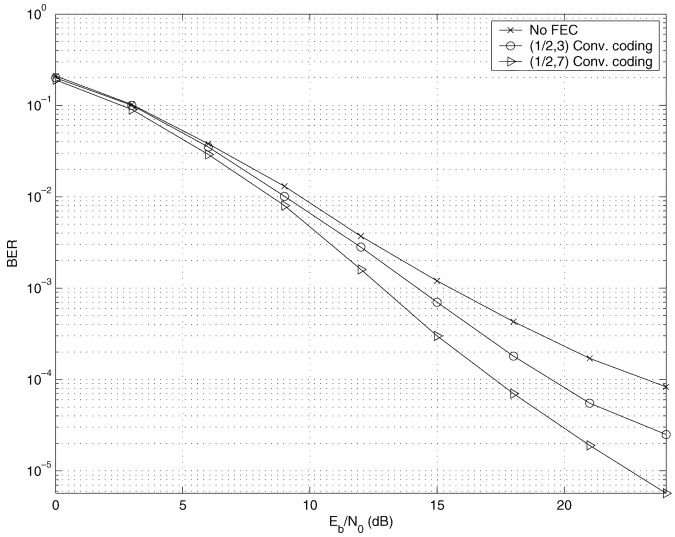

Fig. 7. BER versus E_b/N_0 for quasi-orthogonal ST-OFDM systems with different FEC schemes ($N_s = 128$, $v_s = 30$ km/h, $T_s = 5 \times 10^{-7}$ s).

with, error floors are observed for all of them. To effectively cancel the error floor, the receiver schemes must deal with both ICI and ITAI. The frequency-domain correlative coding [28] combined with a sequential nulling and cancellation process [29] could be one of such schemes, but discussions of its details are beyond the scope of this paper.

As a result of dividing the total bandwidth into many narrowband subcarriers, each subcarrier in an OFDM system suffers from flat fading, and system performance degradation is dominated by the weakest subcarrier. To protect data against deep fades an individual subcarrier may experience, an effective technique is to employ forward error correction (FEC) codes, which is often combined with an interleaver before modulation of input data onto subcarriers. This will effectively spread the same information bit onto many subcarriers which may experience fading of low correlations. The receiver must perform channel decoding after the normal detector (e.g., the ZF or MMSE detector). Fig. 7 shows the simulated BER curves of the quasi-orthogonal ST-OFDM system with rate-1/2 convolutional codes of different constraint lengths (three and seven). $N_s = 128$ is adopted, and all other parameters are the same as those applied for Fig. 4. Although, as expected, the outer channel encoding improves system performance, there is still a need of other techniques to effectively eliminate the error floor caused by time-selective fading.

We have assumed perfect CSI for all numerical results so far. In practical systems, however, there exist channel-estimation errors. It is beyond the scope of this paper to discuss channel-estimation schemes for time-varying fading channels. To assess its impact, channel-estimation error is emulated by introducing an error with a normalized average mean-square error (MSE) defined as $\text{MSE} = E[\|\hat{\boldsymbol{H}} - \boldsymbol{H}\|_F^2]/E[\|\boldsymbol{H}\|_F^2]$. The performance results of quasi-orthogonal ST-OFDM systems with various MSE values are shown in Fig. 8, where $N_s = 64$ and other parameters are the same as those applied in Fig. 4. It is observed that when the MSE value of channel-estimation errors is small (e.g., 10^{-3}), the performance degradation is negligible.

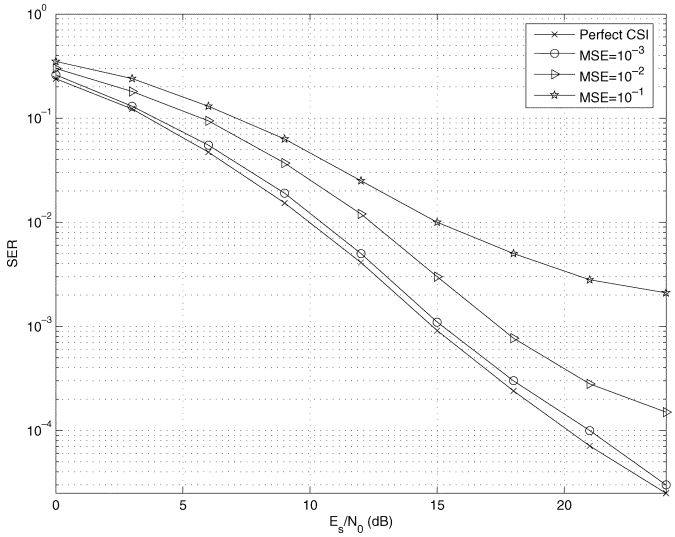

Fig. 8. SER versus E_s/N_0 for quasi-orthogonal ST-OFDM systems with different MSE ($N_s = 64$, $v_s = 30$ km/h, $T_s = 5 \times 10^{-7}$ s).

V. Conclusion

We have analyzed the impact of channel time selectivity on the performance of quasi-orthogonal STC OFDM systems. Specifically, we have quantified ICI and evaluated ITAI caused by channel time variations. Performances of five detection schemes are compared, and it seems that none of them can effectively eliminate the error floor of ST-OFDM in a time-selective environment. It is also observed that an increase in Doppler shift, symbol duration, or number of OFDM subcarriers lowers the achievable CIR. With a symbol duration of $T_s = 5 \times 10^{-7}$ s and a small N_s (e.g., 12), system SER performance is quite insensitive to changes in vehicle speeds and the channel power-delay profile. However, with the same T_s and even a low vehicle speed (e.g., 30 km/h), SER performance is very sensitive to changes in the number of subcarriers.

Appendix
Proof That $\boldsymbol{\Upsilon}$ is a Circulant Matrix

Since $\boldsymbol{\Upsilon}$ in (27) is the same for any antenna index p, we can replace vector $\boldsymbol{h}_l(n)$ of the channel matrix $\boldsymbol{H}$ in (6) with a scalar $h_{p,l}(n)$ (note that the OFDM symbol index is omitted for notation simplicity), forming a new $N_s \times N_s$ matrix given in (40) at the bottom of the page. Let us also define

$$\begin{aligned}\boldsymbol{\mathcal{G}} &= \{g_{ij}^{(p)},\ i,j = 0,\ldots,N_s-1\} = \boldsymbol{U}\boldsymbol{\mathcal{H}}\boldsymbol{U}^H \\ \boldsymbol{\Upsilon} &= \{\gamma_{ij}^{(p)}\} = \{\mathrm{var}(g_{ij}^{(p)})\}\end{aligned} \tag{41}$$

where $\boldsymbol{U}$ is the DFT matrix defined in (5). We note that $\boldsymbol{U} = \{u_{ij}\} = [\boldsymbol{u}_0,\ldots,\boldsymbol{u}_{N_s-1}]$, where $u_{ij} = (1/\sqrt{N_s})e^{-(2\pi\sqrt{-1}/N_s)ij}$. Since $\boldsymbol{\Upsilon}$ is independent of p, we omit antenna index p in the following discussion. If we denote $\boldsymbol{\mathcal{H}}$ as the sum of L matrices $\boldsymbol{\mathcal{H}} = \sum_{l=0}^{L-1}\boldsymbol{\mathcal{H}}_{[l]}$, where $\boldsymbol{\mathcal{H}}_{[l]}$ is a matrix formed by cyclic left-shifting the diagonal matrix $\mathrm{diag}\{h_l(0),\ldots,h_l(N_s-1)\}$ by l columns, we have

$$\boldsymbol{\mathcal{G}} = \boldsymbol{U}\boldsymbol{\mathcal{H}}\boldsymbol{U}^H = \sum_{l=0}^{L-1}\boldsymbol{\mathcal{G}}_l = \sum_{l=0}^{L-1}\boldsymbol{U}\boldsymbol{\mathcal{H}}_{[l]}\boldsymbol{U}^H \tag{42}$$

where $\boldsymbol{\mathcal{G}}_l = \{g_{l,ij}\}$. Because

$$\begin{aligned}E[h_l(n)] &= 0,\ l = 0,\ldots,L-1,\ n = 0,\ldots,N_s-1 \\ E[h_l(r)\cdot h_{l'}^*(s)] &= J_0(2\pi|r-s|f_dT_s)\delta_{l-l'}e^{-\tau_l/\tau_{\mathrm{rms}}}, \\ & \qquad r,s = 0,\ldots,N_s-1\end{aligned} \tag{43}$$

it is easy to recognize that $\boldsymbol{\Upsilon} = \sum_{l=0}^{L-1}\boldsymbol{\Upsilon}_l$, where $\boldsymbol{\Upsilon}_l = \{\gamma_{l,ij}\} = \{\mathrm{var}(g_{l,ij})\}$. Since the sum of circulant matrices of the same dimension is also a circulant matrix, we only need to prove that each $\boldsymbol{\Upsilon}_l$ is a circulant matrix.

For any integer n, let $[n]$ denote n modulo N_s, i.e., $[n]$ is the remainder from dividing n by N_s. Then $g_{l,ij}$ is obtained as

$$\begin{aligned}g_{l,ij} &= \boldsymbol{u}_i^T\boldsymbol{\mathcal{H}}_{[l]}\boldsymbol{u}_j^* \\ &= \sum_{n=0}^{N_s-1}u_{in}u_{j,[n-l]}^*h_l(n) \\ &= \boldsymbol{\eta}_{ij}^T\boldsymbol{h}_l\end{aligned} \tag{44}$$

where $\boldsymbol{\eta}_{ij} = [\eta_{ij0},\ldots,\eta_{ij,(N_s-1)}]^T$, $\eta_{ijn} = u_{in}u_{j,[n-l]}^*$, and $\boldsymbol{h}_l = [h_l(0),\ldots,h_l(N_s-1)]^T$. Thus

$$\begin{aligned}\gamma_{l,ij} &= \mathrm{var}(g_{l,ij}) = \mathrm{var}(\boldsymbol{\eta}_{ij}^T\boldsymbol{h}_l) \\ &= \boldsymbol{\eta}_{ij}^T\mathrm{cov}(\boldsymbol{h}_l)\boldsymbol{\eta}_{ij}^* \\ &= \sum_{r=0}^{N_s-1}\sum_{s=0}^{N_s-1}\eta_{ijr}\chi(r,s)\eta_{ijs}^* \\ &= \sum_{r=0}^{N_s-1}\sum_{s=0}^{N_s-1}\chi(r,s)u_{ir}u_{j,[r-l]}^*u_{is}^*u_{j,[s-l]} \\ &= \frac{1}{N_s^2}\sum_{r=0}^{N_s-1}\sum_{s=0}^{N_s-1}\chi(r,s)e^{-(2\pi\sqrt{-1}/N_s)t_{ijrs}}\end{aligned} \tag{45}$$

$$\boldsymbol{\mathcal{H}} = \begin{bmatrix} h_{p,0}(0) & \cdots & 0 & h_{p,L-1}(0) & \cdots & h_{p,1}(0) \\ \vdots & & & \vdots & & \vdots \\ h_{p,L-1}(L-1) & \cdots & h_{p,1}(L-1) & h_{p,0}(L-1) & \cdots & 0 \\ \vdots & & & \vdots & & \vdots \\ 0 & \cdots & h_{p,L-1}(N_s-1) & \cdots & h_{p,1}(N_s-1) & h_{p,0}(N_s-1) \end{bmatrix} \tag{40}$$

$$\begin{aligned}\gamma_{ij} &= \sum_{l=0}^{L-1} \gamma_{l,ij} \\ &= \frac{1}{N_s^2} \sum_{l=0}^{L-1} \sum_{r=0}^{N_s-1} \sum_{s=0}^{N_s-1} J_0(2\pi|r-s|f_d T_s) \times e^{-(2\pi\sqrt{-1}/N_s)t_{ijrs}} e^{-\tau_l/\tau_{\rm rms}} \\ &= \frac{1}{N_s^2} \sum_{l=0}^{L-1} \left[N_s + 2 \sum_{m=1}^{N_s-1} (N_s - m) J_0(2\pi m f_d T_s) \times \cos\left(\frac{2\pi}{N_s}[j-i]m\right) \right] e^{-\tau_l/\tau_{\rm rms}} \end{aligned} \tag{46}$$

where $\mathrm{cov}(\cdot)$ denotes covariance, $\chi(r,s) = \mathrm{cov}(h_l(r) \cdot h_l^*(s))$, and $t_{ijrs} = ir - j[r-l] - is + j[s-l]$. It suffices to show, for any fixed r and s, that $[t_{ijrs}] = [ir - j[r-l] - is + j[s-l]] = [j-i][s-r]$.

Also note that an $N_s \times N_s$ matrix $\boldsymbol{B} = \{b_{ij}\}, 0 \le i, j \le N_s - 1$, is circulant if and only if $b_{ij} = \kappa_{[j-i]}$, i.e., if and only if b_{ij} depends only on $[j-i]$ and $e^{-(2\pi\sqrt{-1}/N_s)k} = e^{-(2\pi\sqrt{-1}/N_s)[k]}$ because $e^{2\pi\sqrt{-1}} = 1$. Thus, from (45), we can conclude that $\boldsymbol{\Upsilon}_l$ is a circulant matrix if $h_l(n), n = 0, \ldots, N_s - 1$, are finite.

Moreover, from (45), we have (46), shown at the top of the page.

ACKNOWLEDGMENT

The authors would like to thank Professor D. S. Birkes for his help with the proof in the Appendix.

REFERENCES

[1] M. Russell and G. J. Stüber, "Interchannel interference analysis of OFDM in a mobile environment," in *Proc. IEEE Veh. Technol. Conf.*, 1995, pp. 820–824.

[2] J. Li and M. Kavehrad, "Effects of time selective multipath fading on OFDM systems for broadband mobile applications," *IEEE Commun. Lett.*, vol. 3, no. 12, pp. 332–334, Dec. 1999.

[3] V. Tarokh, N. Seshadri, and A. R. Calderbank, "Space-time codes for high data rate wireless communication: Performance criterion and code construction," *IEEE Trans. Inf. Theory*, vol. 44, no. 3, pp. 744–765, Mar. 1998.

[4] S. M. Alamouti, "A simple transmit diversity technique for wireless communications," *IEEE J. Sel. Areas Commun.*, vol. 16, no. 10, pp. 1451–1458, Oct. 1998.

[5] V. Tarokh, H. Jafarkhani, and A. R. Calderbank, "Space-time block codes from orthogonal designs," *IEEE Trans. Inf. Theory*, vol. 45, no. 7, pp. 1456–1467, Jul. 1999.

[6] H. Jafarkhani, "A quasi-orthogonal space–time block code," *IEEE Trans. Commun.*, vol. 49, no. 1, pp. 1–4, Jan. 2001.

[7] O. Tirkkonen, A. Boariu, and A. Hottinen, "Minimal nonorthogonality rate 1 space-time block code for 3+ tx antennas," in *Proc. IEEE ISSSTA*, Sep. 2000, pp. 429–432.

[8] W. Su and X. Xia, "Quasi-orthogonal space-time block codes with full diversity," in *Proc. IEEE GLOBECOM*, Nov. 2002, pp. 1098–1102.

[9] N. Sharma and C. Papadias, "Improved quasi-orthogonal codes through constellation rotation," *IEEE Trans. Commun.*, vol. 51, no. 3, pp. 332–335, Mar. 2003.

[10] W. Lee, C. Sung, and I. Lee, "Channel equalization technique for space–time block codes in non quasi-static channels," in *Proc. IEEE Veh. Technol. Conf.*, 2004, pp. 2215–2219.

[11] T. A. Tran and A. B. Sesay, "A generalized simplified ML decoder of orthogonal space-time block code for wireless communications over time-selective fading channels," in *Proc. IEEE Veh. Technol. Conf.*, 2002, pp. 1911–1915.

[12] F. C. Zheng and A. G. Burr, "Receiver design for orthogonal space-time block coding for four transmit antennas over time-selective fading channels," in *Proc. IEEE GLOBECOM*, Nov. 2003, pp. 128–132.

[13] ——, "Signal detection for nonorthogonal space-time block coding over time-selective fading channels," *IEEE Commun. Lett.*, vol. 8, no. 8, pp. 491–493, Aug. 2004.

[14] G. J. Stüber, J. R. Barry, S. W. Mclaughlin, Y. Li, M. A. Ingram, and T. G. Pratt, "Broadband MIMO-OFDM wireless communications," *Proc. IEEE*, vol. 92, no. 2, pp. 271–294, Feb. 2004.

[15] M. Uysal, N. AL-Dhahir, and C. N. Georghiades, "A space-time block-coded OFDM scheme for unknown frequency-selective fading channels," *IEEE Commun. Lett.*, vol. 5, no. 10, pp. 393–395, Oct. 2001.

[16] Z. Liu, Y. Xin, and G. B. Giannakis, "Space-time-frequency coded OFDM over frequency-selective fading channels," *IEEE Trans. Signal Process.*, vol. 50, no. 10, pp. 2465–2476, Oct. 2002.

[17] A. Stamoulis, S. N. Diggavi, and N. Al-Dhahir, "Intercarrier interference in MIMO OFDM," *IEEE Trans. Signal Process.*, vol. 50, no. 10, pp. 2451–2464, Oct. 2002.

[18] S. Verdú, *Multiuser Detection*. Cambridge, U.K.: Cambridge Univ. Press, 1998.

[19] A. Duel-Hallen, "Decorrelating decision-feedback multiuser detector for synchronous code-division multiple-access channel," *IEEE Trans. Commun.*, vol. 41, no. 2, pp. 285–290, Feb. 1993.

[20] J. Cioffi, G. Dudevoir, M. Eyuboglu, and G. D. Forney, Jr., "MMSE decision feedback equalization and coding—Parts I and II," *IEEE Trans. Commun.*, vol. 43, no. 10, pp. 2582–2604, Oct. 1995.

[21] O. Edfors, M. Sandell, J. -J. v. d. Beek, S. K. Wilson, and P. O. Börjesson, "OFDM channel estimation by singular value decomposition," *IEEE Trans. Commun.*, vol. 46, no. 7, pp. 931–939, Jul. 1998.

[22] R. H. Clarke, "A statistical theory of mobile radio reception," *Bell Syst. Tech. J.*, vol. 47, pp. 957–1000, Jul. 1968.

[23] S. Coleri, M. Ergen, and A. Bahai, "Channel estimation techniques based on pilot arrangement in OFDM systems," *IEEE Trans. Broadcast.*, vol. 48, no. 3, pp. 223–229, Sep. 2002.

[24] O. Simeone, Y. Bar-Ness, and U. Spagnolini, "Pilot-based channel estimation for OFDM systems by tracking the delay-subspace," *IEEE Trans. Wireless Commun.*, vol. 3, no. 1, pp. 315–325, Jan. 2004.

[25] H. Moose, "A technique for orthogonal frequency-division multiplexing frequency offset correction," *IEEE Trans. Commun.*, vol. 42, no. 10, pp. 2908–2914, Oct. 1994.

[26] A. Klein, G. K. Kaleh, and P. W. Baier, "Zero forcing and minimum mean-square error equalization for multiuser detection in code-division multiple-access channels," *IEEE Trans. Veh. Technol.*, vol. 45, no. 3, pp. 276–287, May 1996.

[27] A. Duel-Hallen, "Equalizers for multiple input/multiple output channels and PAM systems with cyclostationary input sequences," *IEEE J. Sel. Areas Commun.*, vol. 10, no. 4, pp. 630–639, Apr. 1992.

[28] Y. Zhao and S. G. Häggman, "Intercarrier interference compression in OFDM communication systems by using correlative coding," *IEEE Commun. Lett.*, vol. 2, no. 8, pp. 214–216, Aug. 1998.

[29] B. Hassibi, "A fast square-root implementation for BLAST," in *Proc. 34th Asilomar Conf. Signals, Syst., Comput.*, Pacific Grove, CA, Oct. 2000, pp. 1255–1259.

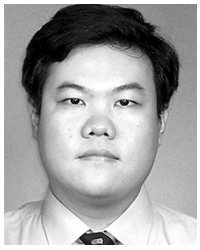

Yu Zhang (S'05) received the B.E. and M.S. degrees, both in electronic engineering, from Tsinghua University, Beijing, China, in 1999 and 2002, respectively. He is currently working toward the Ph.D. degree in the school of Electrical Engineering and Computer Science, Oregon State University, Corvallis.

His current research interests include performance analysis and detection schemes for MIMO-OFDM systems over doubly selective fading channels, transmitter and receiver diversity techniques, and channel estimation and equalization algorithms.

Huaping Liu (S'95–M'97) received the B.S. and M.S. degrees from Nanjing University of Posts and Telecommunications, Nanjing, China, in 1987 and 1990, respectively, and the Ph.D. degree from New Jersey Institute of Technology, Newark, in 1997, all in electrical engineering.

From July 1997 to August 2001, he was with Lucent Technologies, NJ. Since September 2001, he has been an Assistant Professor with the School of Electrical Engineering and Computer Science, Oregon State University, Corvallis. His research interests include capacity and performance analysis of wireless systems, communication techniques for multiuser time-varying environments with applications to cellular and indoor wireless communications, ultra-wideband schemes, and MIMO OFDM systems.